

# Mean-field regime of trapped dipolar Bose-Einstein condensates in one and two dimensions

Yongyong Cai,<sup>1</sup> Matthias Rosenkranz,<sup>1,\*</sup> Zhen Lei,<sup>2,3,4</sup> and Weizhu Bao<sup>1,5,†</sup>

<sup>1</sup>Department of Mathematics, National University of Singapore, 119076, Singapore

<sup>2</sup>School of Mathematical Sciences, Fudan University, Shanghai 200433, China

<sup>3</sup>Key Laboratory of Nonlinear Mathematical Models and Methods of Ministry of Education, Fudan University, Shanghai 200433, China

<sup>4</sup>Shanghai Key Laboratory for Contemporary Applied Mathematics, Fudan University, Shanghai 200433, China

<sup>5</sup>Center for Computational Science and Engineering, National University of Singapore, 117543, Singapore

(Dated: May 29, 2018)

We derive rigorous one- and two-dimensional mean-field equations for cigar- and pancake-shaped dipolar Bose-Einstein condensates with arbitrary polarization angle. We show how the dipolar interaction modifies the contact interaction of the strongly confined atoms. In addition, our equations introduce a nonlocal potential, which is anisotropic for pancake-shaped condensates. We propose to observe this anisotropy via measurement of the condensate aspect ratio. We also derive analytically approximate density profiles from our equations. Both the numerical solutions of our reduced mean-field equations and the analytical density profiles agree well with numerical solutions of the full Gross-Pitaevskii equation while being more efficient to compute.

PACS numbers: 03.75.Hh, 75.80.+q, 67.85.-d

## I. INTRODUCTION

Quantum-degenerate gases with long-range interactions have received much attention recently both from experimental and theoretical studies. In conventional experiments with bosonic quantum gases, short-range interactions have played a leading role and are well described by the s-wave scattering length [1]. With the realization of a dipolar chromium Bose-Einstein condensate (BEC) it is now possible to go beyond such isotropic interactions in degenerate gases [2, 3]. Dipolar interactions have a long-range and anisotropic component. These features crucially affect the ground state properties [4, 5], stability [6, 7], and dynamics of the gas [8]. Furthermore, they offer a route for studying exciting many-body quantum effects such as a superfluid-crystal quantum phase transition [9], supersolids [10] or even topological order [11] (for a review of the experimental and theoretical progress in dipolar gases see Refs. [12, 13]).

<sup>52</sup>Cr possess a comparatively large magnetic dipole moment of 6 Bohr magnetons. A large magnetic dipole moment makes atomic BECs an ideal candidate for studying the interplay between contact and dipole-dipole interactions. By reducing the s-wave scattering length via a Feshbach resonance it is even possible that dipole-dipole interactions dominate the properties of the BEC [14, 15]. Dipolar effects have also been observed in a spinor alkali condensate [16]. Furthermore, dc electric fields can induce large electric dipole moments in alkali atoms [17]. Systems with a large permanent electric dipole moment include heteronuclear molecules [18, 19], which are harder to cool to quantum degeneracy [20, 21], and Rydberg atoms [22].

Complementing the tremendous experimental progress, many properties of trapped dipolar BECs have been investigated theoretically. The Gross-Pitaevskii equation (GPE)

with a nonlocal potential determines its ground state density profile in three dimensions and at zero temperature [5]. Neglecting the kinetic energy term, O'Dell *et al.* [23], Eberlein *et al.* [24] have shown that, remarkably, the ground state density profile of a harmonically trapped three-dimensional (3D) dipolar BEC is an inverted parabola just as in the nondipolar BEC. On the other hand, in most experiments to date a strong harmonic trap (or optical lattice) along one or two axes confines the dipolar BEC to a cigar or pancake shape, respectively [3, 15]. For these cases, Parker and O'Dell [25] have derived one- (1D) and two-dimensional (2D) density profiles of a dipolar BEC both in the Thomas-Fermi (TF) limit and the 1D and 2D mean-field limit. However, their results are only valid for polarization along the symmetry axis. Several authors have derived effective dipolar potentials in lower dimensions for either axial or transverse polarizations [26–31]. To our knowledge, an effective dipolar potential valid for arbitrary polarization direction of quasi-1D and quasi-2D dipolar BECs has not been proposed yet.

Apart from a conceptual clarity, effective equations for lower dimensional dipolar BECs also offer a clear advantage for numerical computations. For strong trap anisotropies the time scales along the compressed and elongated axes are very different, which makes an accurate numerical treatment hard. Instead of solving the full 3D problem, it is hence desirable to

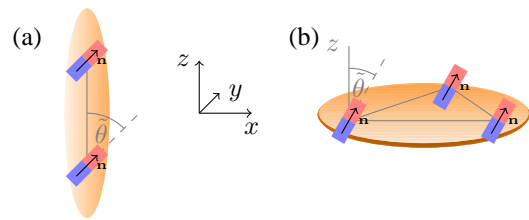


FIG. 1. (Color online) In the quasi-1D setup in (a) the dipolar BEC is confined to the  $z$  direction. In the quasi-2D setup in (b) the atoms are confined to the  $x$ - $y$  plane. The dipoles are polarized along the axis  $\mathbf{n} = (n_x, n_y, n_z)$  with polar angle  $\hat{\theta}$  (i.e.,  $n_z = \cos \hat{\theta}$ ).

\* matrm@nus.edu.sg

† bao@math.nus.edu.sg; <http://www.math.nus.edu.sg/~bao/>

find governing equations for lower dimensional dipolar BECs which are suitable for efficient numerical methods. This is particularly important for very strong confinement or low densities, where the usual TF approximation for the full 3D GPE becomes invalid [1].

In this paper, we present mean-field equations for trapped dipolar BECs in one and two dimensions polarized along an arbitrary axis. Our equations are based on a mathematically rigorous dimension reduction of the 3D Gross-Pitaevskii equation (GPE) to lower dimensions. For BECs without dipolar interactions the formal analysis [32–34] and rigorous analysis [35–38] of such a dimension reduction has been discussed extensively in the physical and mathematical literature. On the other hand, only few mathematically rigorous results are available for the dimension reduction of dipolar BECs, such as Ref. [39]. The main advantages of our effective equations over previously derived results are: (i) valid for arbitrary dipole alignment, (ii) well amenable for efficient numerical computations typically based on the Fourier transformation and related methods.

For the derivation of the 1D (2D) case we assume that the BEC is in the ground state of the radial (axial) trap (see Fig. 1). We find that the ground state of the lower-dimensional dipolar BEC is determined by a modified contact interaction term and a nonlocal potential. Compared to a confined BEC with only s-wave interactions here the contact interaction also depends on the strength of the dipolar interaction and the  $z$ -component of the polarization axis. Crucially, it is independent of the transverse components of the polarization. In 2D the nonlocal term introduces anisotropy in the BEC ground state density, which can be measured, *e.g.*, in time-of-flight experiments as a modified aspect ratio of the BEC [3, 40]. We discuss the aspect ratio of the BEC for the intermediate regime between the special cases of parallel and orthogonal polarization, which have been studied before [23, 25]. Furthermore, we present simple analytical density profiles in 1D and 2D derived from our mean-field equations. We compare ground states of the quasi-1D and quasi-2D BEC at different polarizations with the ground states of the full 3D BEC and find good agreement. In particular, our ground states are a good approximation to the ground states of the full GPE in regimes where the TF approximation fails. In the limit of strong axial confinement we can cast our nonlocal potential into a form similar to the Poisson equation found for 3D dipolar BECs [23].

This paper is organized as follows. In Sec. II, we introduce the model of a 3D dipolar BEC at zero temperature. As our first main result, in Sec. III we present a mean-field equation for a quasi-1D dipolar BEC. We compare the ground state solutions of this 1D equation with the full 3D computation and an approximate analytical solution. In Sec. IV, we present our second main result, namely, a mean-field equation for a quasi-2D dipolar BEC. Again we compare its solutions to the 3D GPE solution and our analytical approximation. Moreover, we calculate the aspect ratio of the BEC if the polarization of the dipoles is changed continuously from the longitudinal to a radial axis. We conclude in Sec. V. In Appendix A and B we present details of the dimension reduction from the 3D GPE to the 1D and 2D mean-field equations, respectively. In Ap-

pendix C we derive closed forms for the nonlocal potentials in 1D and 2D for arbitrary dipole alignment.

## II. 3D MODEL

We consider a dilute dipolar BEC at zero temperature trapped in a harmonic potential  $V(\mathbf{r}) = \frac{m}{2}(\omega_x^2 x^2 + \omega_y^2 y^2 + \omega_z^2 z^2)$ , where  $m$  is the particle mass and  $\omega_{x,y,z}$  are the trap frequencies. We focus on atomic BECs with a magnetic dipole moment but it is straightforward to extend the analysis to degenerate bosonic gases with electric dipole moments. We assume that the atoms are polarized along a dipolar axis  $\mathbf{n} = (n_x, n_y, n_z)$  with  $\sum_i n_i^2 = 1$ . Away from shape resonances, the wave function  $\psi(\mathbf{r}, t)$  of the gas is governed by the GPE [5, 17, 41]

$$i\hbar\partial_t\psi(\mathbf{r}, t) = \left[ -\frac{\hbar^2}{2m}\nabla^2 + V(\mathbf{r}) + g|\psi|^2 + \Phi_{dd} \right] \psi(\mathbf{r}, t), \quad (1)$$

where  $g = 4\pi\hbar^2 a_s/m$  is the contact interaction strength with s-wave scattering length  $a_s$ . The dipolar potential  $\Phi_{dd}$  is given by the convolution

$$\Phi_{dd} = \int d^3\mathbf{r}' U_{dd}(\mathbf{r} - \mathbf{r}') |\psi(\mathbf{r}', t)|^2 \quad (2)$$

with the dipole interaction

$$U_{dd}(\mathbf{r}) = \frac{C_{dd}}{4\pi} \frac{1 - 3\cos^2\theta}{|\mathbf{r}|^3}. \quad (3)$$

Here,  $\theta$  is the angle between the polarization axis  $\mathbf{n}$  and the relative position of two atoms (*i.e.*,  $\cos\theta = \mathbf{n} \cdot \mathbf{r}/|\mathbf{r}|$ ). For magnetic dipoles we have  $C_{dd} = \mu_0\mu_d^2$ , where  $\mu_0$  is the magnetic vacuum permeability and  $\mu_d$  the dipole moment, and for electric dipoles we have  $C_{dd} = d^2/\epsilon_0$ , where  $\epsilon_0$  is the vacuum permittivity and  $d$  the electric dipole moment. We note that it is possible to modify the dipolar interaction  $C_{dd}$  by means of a rotating magnetic field [42].

We use a mathematical identity to write the dipole interaction Eq. (3) as [23, 43]

$$U_{dd}(\mathbf{r}) = -C_{dd} \left( \frac{1}{3}\delta(\mathbf{r}) + \partial_{\mathbf{nn}} \frac{1}{4\pi|\mathbf{r}|} \right). \quad (4)$$

Here we denote with  $\partial_{\mathbf{n}} = n_x\partial_x + n_y\partial_y + n_z\partial_z$  the derivative along the dipole axis and  $\partial_{\mathbf{nn}} = \partial_{\mathbf{n}}(\partial_{\mathbf{n}})$ . Inserting Eq. (4) and Eq. (2) into the GPE, Eq. (1), results in

$$i\hbar\partial_t\psi = \left[ -\frac{\hbar^2}{2m}\nabla^2 + V(\mathbf{r}) + \left( g - \frac{C_{dd}}{3} \right) |\psi|^2 + \tilde{\Phi}_{3D} \right] \psi. \quad (5)$$

We note that two terms contribute to the dipolar interaction. The first term in Eq. (4) reduces the contact interaction strength [third term in Eq. (5)], while the second term in Eq. (4) contributes the potential  $\tilde{\Phi}_{3D} = -C_{dd}\partial_{\mathbf{nn}} \int d^3\mathbf{r}' U_{3D}(\mathbf{r} - \mathbf{r}') |\psi(\mathbf{r}', t)|^2$  with kernel  $U_{3D}(\mathbf{r}) = 1/4\pi|\mathbf{r}|$ .

We introduce dimensionless quantities by rescaling lengths with  $\mathbf{r} \rightarrow \mathbf{r}a_0$ , times with  $t \rightarrow t/\omega_0$ , energies with  $\hbar\omega_0$ , and the wave function with  $\psi \rightarrow \psi\sqrt{N/a_0^3}$ , where  $\omega_0$  is the smallest trap frequency in the system [ $\omega_0 = \min(\omega_x, \omega_y, \omega_z)$ ],  $a_0 = \sqrt{\hbar/m\omega_0}$  the corresponding magnetic length, and  $N$  the total number of atoms in the BEC. After rescaling, in dimensionless form Eq. (5) is given by

$$i\partial_t\psi = \left[ -\frac{1}{2}\nabla^2 + V(\mathbf{r}) + \beta(1 - \epsilon_{dd})|\psi|^2 + \Phi_{3D} \right] \psi, \quad (6a)$$

$$\Phi_{3D} = -3\beta\epsilon_{dd}\partial_{\mathbf{nn}} \int d^3\mathbf{r}' U_{3D}(\mathbf{r} - \mathbf{r}') |\psi(\mathbf{r}', t)|^2. \quad (6b)$$

where  $\beta = 4\pi N a_s/a_0$  and  $\epsilon_{dd} = C_{dd}/3g$  defines a natural dimensionless parameter for the relative strength of dipolar and s-wave interactions. The dimensionless trapping potential is  $V(\mathbf{r}) = \frac{1}{2}(\gamma_x^2 x^2 + \gamma_y^2 y^2 + \gamma_z^2 z^2)$  with  $\gamma_x = \omega_x/\omega_0$ ,  $\gamma_y = \omega_y/\omega_0$ ,  $\gamma_z = \omega_z/\omega_0$ .

### III. QUASI-1D DIPOLAR BEC

By choosing a sufficiently large radial trap frequency it is possible to freeze the radial motion of the BEC [44]. If the extent of the radial cloud is much larger than the s-wave scattering length, this is the limit of a quasi-1D BEC [45]. In Fig. 1(a) we illustrate the geometry of this setup. In this sec-

tion, we present an intuitive mean-field equation for the axial wave function of such a strongly confined dipolar BEC. Our equation is based on a reduction of the 3D GPE to 1D assuming a strong radial confinement.

#### A. 1D mean-field equation

In order to derive a mean-field equation for the axial wave function of the condensate we assume that  $\omega_z \ll \omega_x = \omega_y =: \omega_\perp$  and  $gn_0 \ll \hbar\omega_\perp$ , where  $n_0$  is the peak density of the BEC. Moreover, we require that dipole interactions do not excite radial modes, *i.e.*,  $\Phi_{dd} \ll \hbar\omega_\perp$ . Then the radial modes of the BEC are in the ground state of the transversal harmonic trap and the order parameter  $\psi$  of the BEC factorizes. We write the factorized wave function as

$$\psi(\mathbf{r}, t) = e^{-i\omega_\perp t} w_{2D}(x, y) \psi_{1D}(z, t), \quad (7)$$

$$w_{2D}(x, y) = \sqrt{\frac{m\omega_\perp}{\pi\hbar}} e^{-m\omega_\perp(x^2+y^2)/2\hbar}. \quad (8)$$

In this section we rescale equations in terms of the dimensionless lengths  $\mathbf{r} \rightarrow \mathbf{r}a_z$ , times  $t \rightarrow t/\omega_z$ , and the axial wave function  $\psi_{1D} \rightarrow \psi_{1D}\sqrt{N/a_z}$  with  $a_z = \sqrt{\hbar/m\omega_z}$  the magnetic length in  $z$  direction. Energies are expressed in units of  $\hbar\omega_z$ . Given these assumptions, in Appendix A we show that the 3D GPE, Eq. (1), reduces to an equation for the axial wave function  $\psi_{1D}$

$$i\partial_t\psi_{1D}(z, t) = \left\{ -\frac{1}{2}\partial_{zz} + V_{1D}(z) + \frac{\beta_{1D}\gamma}{2\pi} \left[ 1 + \frac{\epsilon_{dd}}{2} (1 - 3n_z^2) \right] |\psi_{1D}(z, t)|^2 + \Phi_{1D} \right\} \psi_{1D}(z, t), \quad (9a)$$

$$\Phi_{1D} = \frac{3\beta_{1D}\epsilon_{dd}\sqrt{\gamma}}{8\sqrt{2\pi}} (1 - 3n_z^2) \partial_{zz} \int_{-\infty}^{\infty} dz' U_{1D}(z - z') |\psi_{1D}(z', t)|^2, \quad (9b)$$

where  $V_{1D}(z) = z^2/2$ ,  $\beta_{1D} = gN/\hbar\omega_z a_z^3 = 4\pi N a_s/a_z$  and  $n_z$  is the  $z$  component of the dipole axis  $\mathbf{n}$ . The trap aspect ratio is given by  $\gamma = \omega_\perp/\omega_z$ . We find for the kernel  $U_{1D}$

$$U_{1D}(z) = e^{\gamma z^2/2} \operatorname{erfc}(|z|\sqrt{\gamma/2}), \quad (10)$$

where  $\operatorname{erfc}$  is the complementary error function. In Appendix C we calculate the derivative in Eq. (9b) and give a closed form of the resulting convolution integral. However for our focus on numerical computation of the ground state, expression (9b) is better suited. It is worth pointing out that the only approximation in the derivation of Eq. (9) from the GPE is the factorization in Eq. (7) with the choice of a Gaussian as the radial wave function  $w_{2D}(x, y)$ .

The formula for the wave function of a quasi-1D dipolar BEC, Eq. (9a), is very intuitive. It has the same structure as the corresponding 3D expression Eq. (6a). Notably, the effect of the dipolar interaction in 1D is an altered contact interaction strength and the introduction of a nonlocal potential  $\Phi_{1D}$ . In Fig. 2(a) we plot the kernel  $U_{1D}$  of the potential, Eq. (10),

for different trap aspect ratios. In contrast to the kernel  $U_{3D}$  in 3D, the kernel of the 1D potential does not diverge at the origin. Instead we find  $U_{1D}(z) = 1 - \sqrt{2\gamma}|z|/\sqrt{\pi} + \mathcal{O}(|z|^2)$  for  $|z| \rightarrow 0$ . In the opposite limit,  $|z| \rightarrow \infty$ , we find  $U_{1D}(z) \sim \sqrt{2}/\sqrt{\pi\gamma}|z|$ , *i.e.*, it scales with  $1/|z|$  as the 3D kernel. These properties allow for efficient numerical methods based on Eq. (9) [43].

#### B. Ground state

The third term in Eq. (9a) describes the altered contact interaction, which now depends on the dipolar interaction strength  $\beta_{1D}\epsilon_{dd}$ . The anisotropy of the dipolar interaction is manifest in this term in the dependence on the  $z$  component  $n_z = \cos\theta$  of the dipole axis, where  $\theta$  is the angle between dipole and  $z$  axis [cf. Fig. 1(a)]. If the dipoles are aligned along the longitudinal BEC axis ( $n_z = 1$ ), the effective contact interaction reduces by a factor of  $(1 - \epsilon_{dd})$ . Neglecting the

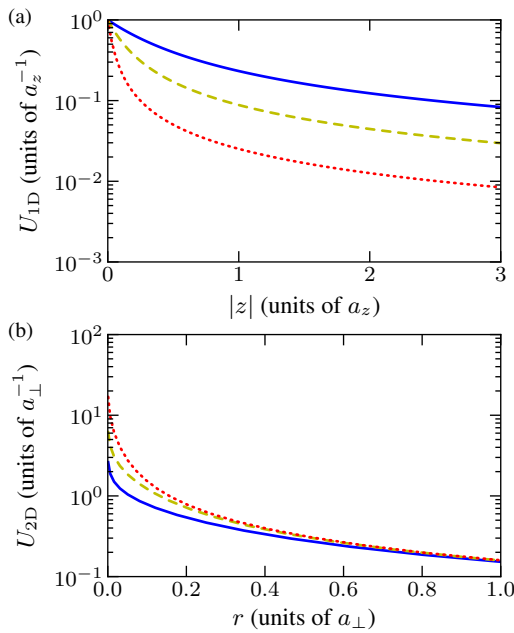


FIG. 2. (a) The kernel  $U_{1D}$ , Eq. (10), for  $\gamma = 10$  (solid line), 80 (dashed), 1000 (dotted). (b)  $U_{2D}$ , Eq. (17), for  $\gamma = 1/10$  (solid),  $1/80$  (dashed),  $1/1000$  (dotted). In both cases increasing the confinement of the BEC leads to increasingly local behavior.

nonlocal part of Eq. (9a) this results in a reduced BEC length. If the dipole axis is perpendicular to the BEC axis ( $n_z = 0$ ), the BEC length increases since the contact interaction is larger by a factor  $(1 + \epsilon_{dd}/2)$ . Intuitively, these two cases can be understood in terms of a string of magnets: magnets with poles aligned head to tail attract each other, while magnets in a head to head or tail to tail configuration repel each other. However, our equation also maps out all intermediate configurations between these two special cases. Finally, we notice the familiar increase of the effective s-wave scattering strength in 1D by a factor  $\gamma/2\pi$ , which is due to the choice of a Gaussian ground state in the factorization Eq. (7) [33, 46].

The potential  $\Phi_{1D}$  in Eq. (9a) describes the nonlocal effect of the dipolar interaction on the BEC. The shape of the kernel  $U_{1D}$  [see Fig. 2(a)] reveals that this potential becomes more local with increasing trap aspect ratio  $\gamma$ . Moreover, for large  $\gamma$  we expect that  $\Phi_{1D}$  does not affect the shape of the BEC significantly. Owing to the properties of convolutions we may apply the second derivative in  $\Phi_{1D}$  only to the density  $|\psi_{1D}|^2$  in the integral. However, for the ground state we expect this density to become flatter for large  $\gamma$  so that the derivative becomes smaller. Since the contact interaction scales linearly with  $\gamma$ , the contact term dominates over the nonlocal potential. Similar to the modified contact interaction our Eq. (9b) explicitly states the dependence of  $\Phi_{1D}$  on the  $z$ -component of the dipole axis (and predicts no dependence on other components).

We have seen that the dipolar interaction in 1D is composed of a local (or contact) interaction and a nonlocal interaction. In order to determine the sign of the

nonlocal interaction, we evaluate the corresponding energy via Fourier transformation. The energy is given by  $\frac{1}{2} \int dz \Phi_{1D} |\psi_{1D}(z, t)|^2 = \frac{1}{2} \int dk_z \widehat{\Phi}_{1D} |\widehat{\psi}_{1D}|^2(k_z, t) = -\frac{3\beta_{1D}\epsilon_{dd}\sqrt{\gamma}}{16} (1 - 3n_z^2) \int dk_z k_z^2 \widehat{U}_{1D}(k_z) \left| \widehat{\psi}_{1D}|^2(k_z, t) \right|^2$ , where  $\widehat{f}(k_z) = (1/\sqrt{2\pi}) \int dz f(z) e^{-ik_z z}$  denotes the Fourier transform of a function  $f$ . Since the Fourier transforms  $\widehat{U}_{1D}$  and  $\left| \widehat{\psi}_{1D}|^2 \right|^2$  are positive (see Appendix A), the sign of the nonlocal potential is opposite the sign of the modification in the contact term  $\frac{\beta_{1D}\epsilon_{dd}\sqrt{\gamma}}{4\pi} (1 - 3n_z^2)$ . This means that the nonlocal potential counteracts the action of the contact term: if the contact term is repulsive, the nonlocal potential becomes attractive and vice versa.

Another useful observation is the following. The BEC ground state is not affected by the presence of dipolar interactions for the “magic angle”  $\cos \theta_m = 1/\sqrt{3}$  [47]. In this case, the 3D dipolar potential  $U_{dd}$  vanishes and accordingly Eq. (9) reduces to the GPE for a quasi-1D BEC without dipolar interaction. This observation could be useful for very sensitive matter wave interferometers, where the dipole interaction dominates the decoherence when the s-wave scattering length has been reduced via a Feshbach resonance [15].

We can derive an analytical solution for the density of the quasi-1D dipolar BEC if the contact interaction term in Eq. (9a) is repulsive and dominates the dynamics [1]. In this case, we neglect the kinetic and nonlocal parts in Eq. (9a). Assuming a stationary solution,  $\psi_{1D}(z, t) = e^{-i\mu_z t} \sqrt{n_{1D}(z)}$ , we find the density profile  $n_{1D}(z) = [\mu_z - (z^2/2)] \left\{ \beta_{1D} \frac{\gamma}{2\pi} \left[ 1 + \frac{\epsilon_{dd}}{2} (1 - 3n_z^2) \right] \right\}^{-1}$ , where  $\mu_z$  is the chemical potential along  $z$ . The density vanishes for  $z \geq Z = \sqrt{2\mu_z}$ . We obtain the halfwidth of the condensate  $Z$  by evaluating the normalization condition  $\int dz n(z) = 1$ , which yields

$$Z = \left\{ \frac{3}{2} \frac{\beta_{1D}\gamma}{2\pi} \left[ 1 + \frac{\epsilon_{dd}}{2} (1 - 3n_z^2) \right] \right\}^{1/3}. \quad (11)$$

Inserting this expression into the density profile gives

$$n_{1D}(z) = \frac{3}{4Z} \left( 1 - \frac{z^2}{Z^2} \right). \quad (12)$$

Parker and O’Dell [25] have derived analytical 1D densities for the special case of dipoles aligned along the  $z$  axis. In this case, we note that our generalized expression Eq. (12) coincides with their density in the limit termed “1D mean-field regime”. Generalizing the criterion for the validity of the mean-field regime in Refs. [25, 48], we see that Eq. (12) is a good approximation for the axial density profile of an elongated dipolar BEC if

$$\frac{\beta_{1D}}{4\pi\sqrt{\gamma}} \left[ 1 + \frac{\epsilon_{dd}}{2} (1 - 3n_z^2) \right] \ll 1. \quad (13)$$

In Fig. 3 we compare the density of the quasi-1D BEC determined via Eq. (9) with the analytical prediction Eq. (12) and the numerical solution for the full 3D GPE in Eq. (1) after integrating over the transversal directions. If the dipole axis points perpendicular to the elongated BEC axis, we cannot distinguish the analytical density from the quasi-1D



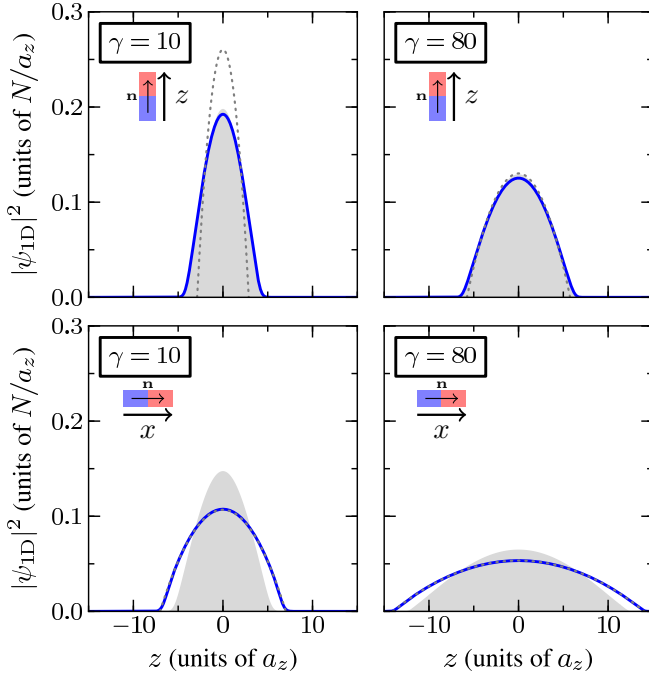


FIG. 3. (Color online) Linear density of the quasi-1D BEC according to the solution of our 2D equation, Eq. (9) (blue solid lines), the corresponding analytical prediction of Eq. (12) (gray dotted), and the full 3D GPE of Eq. (1) (shaded area). In the upper panel dipoles are aligned with the BEC axis, while in the lower panel they are aligned perpendicular to the BEC axis. We choose  $\beta_{1D} = 100$ ,  $\epsilon_{dd} = 0.9$  and the  $\gamma$  given in the plots.

GPE result (see lower panel of Fig. 3). We have checked that for larger values of the trap aspect ratio  $\gamma$  the discrepancy between the full GPE result and our approximate 1D solution with perpendicular dipoles diminishes. On the other hand, if the dipoles are aligned with the BEC axis our 1D mean-field solution agrees very well with the solution of the full GPE (see

upper panel of Fig. 3). Furthermore, we note that the BEC is compressed compared to the case with perpendicular dipole axis. This compression is caused by the attraction of aligned dipoles in a 1D setup, and it is manifest in the reduced contact interaction in Eq. (9a) for  $n_z = 1$ . However, for axial dipoles the nonlocal term in Eq. (9a) produces an appreciable repulsive potential. As a consequence, the BEC is broadened as compared to the analytical profile. Therefore, in the regime of small or moderate interaction energy  $\beta_{1D}$ , we see that the usual approach of neglecting the kinetic and nonlocal terms is not sufficient to describe the density profile. On the other hand, our proposed 1D equation, Eq. (9), describes the BEC accurately in the mean-field regime at experimentally relevant trap aspect ratios  $\gamma$ .

#### IV. QUASI-2D DIPOLAR BEC

In this section we consider a dipolar BEC which is strongly confined along the  $z$  axis, *i.e.*,  $\gamma \ll 1$  [cf. Fig. 1(b)]. Analogous to the preceding section, we assume that  $gn_0 \ll \hbar\omega_z$  and that the axial extent of the cloud is much larger than the  $s$ -wave scattering length. If the dipolar interactions are also small compared to the axial trap energy  $\hbar\omega_z$ , then the BEC is in the ground state of the axial harmonic trap. This is the case of a quasi-2D BEC, where the BEC wave function separates into

$$\psi(\mathbf{r}, t) = e^{-i\omega_z t/2} \psi_{2D}(x, y, t) w_{1D}(z), \quad (14)$$

$$w_{1D}(z) = \left(\frac{m\omega_z}{\pi\hbar}\right)^{1/4} e^{-m\omega_z z^2/2\hbar}. \quad (15)$$

In this section we use the dimensionless rescaling  $\mathbf{r} \rightarrow \mathbf{r}a_{\perp}$ ,  $t \rightarrow t/\omega_{\perp}$ ,  $\psi_{2D} \rightarrow \psi_{2D}\sqrt{N/a_{\perp}^2}$ , where  $a_{\perp} = \sqrt{\hbar/m\omega_{\perp}}$ , is the radial magnetic length. Energies are given in units of  $\hbar\omega_{\perp}$ . We show in Appendix B that the transversal wave function  $\psi_{2D}$  fulfills the following equation

$$i\partial_t \psi_{2D}(x, y, t) = \left\{ -\frac{1}{2} \nabla^2 + V_{2D}(x, y) + \frac{\beta_{2D}}{\sqrt{2\pi}\gamma} [1 - \epsilon_{dd} (1 - 3n_z^2)] |\psi_{2D}(x, y, t)|^2 + \Phi_{2D} \right\} \psi_{2D}(x, y, t), \quad (16a)$$

$$\Phi_{2D} = -\frac{3\beta_{2D}\epsilon_{dd}}{2} [\partial_{\mathbf{n}_{\perp}\mathbf{n}_{\perp}} - n_z^2 \nabla^2] \int dx' dy' U_{2D}(x - x', y - y') |\psi_{2D}(x', y', t)|^2. \quad (16b)$$

Here,  $V_{2D}(x, y) = (x^2 + y^2)/2$  and  $\beta_{2D} = 4\pi N a_s / a_{\perp}$ . We denote with  $\partial_{\mathbf{n}_{\perp}} = n_x \partial_x + n_y \partial_y$  and  $\partial_{\mathbf{n}_{\perp}\mathbf{n}_{\perp}} = \partial_{\mathbf{n}_{\perp}} (\partial_{\mathbf{n}_{\perp}})$ . The kernel  $U_{2D}$  is radially symmetric and is given by

$$U_{2D}(r) = \frac{e^{r^2/4\gamma}}{(2\pi)^{3/2} \sqrt{\gamma}} K_0(r^2/4\gamma), \quad (17)$$

where  $K_{\nu}$  ( $\nu$  real) denotes a modified Bessel function of the second kind and  $r^2 = (x - x')^2 + (y - y')^2$ . In Appendix C we show that the nonlocal potential, Eq. (16b), can be written as a simple convolution  $\Phi_{2D} = -\frac{3\beta_{2D}\epsilon_{dd}}{2} \int dx' dy' U_{2D}^{(\mathbf{n})}(x -$

$x', y - y') |\psi_{2D}(x', y', t)|^2$ . There we also derive a closed form for  $U_{2D}^{(\mathbf{n})}$ , which explicitly depends on the polarization axis. Assuming validity of the GPE, the only approximation in the derivation of Eq. (16) is the factorization Eq. (14).

In Fig. 2(b) we plot the kernel  $U_{2D}$ , Eq. (17), for different trap anisotropies  $\gamma$ . In contrast to the equivalent 1D kernel  $U_{1D}$  in Fig. 2(a), the long range behavior does not depend on  $\gamma$ . In fact, we can show that  $U_{2D}(r) \sim 1/2\pi r$  for  $r \rightarrow \infty$ . This is equivalent to the long-range behavior of the 3D kernel  $U_{3D}$ . However, in the opposite limit,  $r \rightarrow 0$ , we find that

the divergence of the kernel is only logarithmic,  $U_{2D}(r) \simeq \frac{1}{\sqrt{2\pi^3\gamma}}[-\ln(r) + \ln(2\sqrt{\gamma}) + \text{const}]$ .

For numerical computations in Fourier space, the expression Eq. (16b) for the nonlocal potential is often more useful than the closed form derived in Appendix C. Moreover, in the limit of large trap anisotropy,  $\gamma \ll 1$  we have shown that the potential in Eq. (16b) is equivalent to a Poisson-type equation. To this end we introduce the fictitious potential  $\phi_{2D}$  defined by  $\Phi_{2D} = -\frac{3\beta_{2D}\epsilon_{dd}}{2}[\partial_{\mathbf{n}_\perp\mathbf{n}_\perp} - n_z^2\nabla^2]\phi_{2D}$ . For  $\gamma \ll 1$  we may then replace Eq. (16b) by

$$(-\nabla^2)^{1/2}\phi_{2D}(x, y, t) = |\psi_{2D}(x, y, t)|^2. \quad (18)$$

Hence, the computation of the nonlocal potential  $\Phi_{2D}$  in Fourier space involves only multiplications of the density  $|\psi_{2D}|^2$  with the momentum.

In contrast to the 1D mean-field equation, Eq. (9), in 2D the dipolar interaction increases the contact interaction strength for dipoles aligned along the  $z$  axis (and positive  $\epsilon_{dd}$ ). This is a manifestation of the fact that magnets aligned in parallel repel each other. The modification of the contact interaction term by a factor of  $1/\sqrt{2\pi\gamma}$  is due to the compression along the  $z$  axis [33, 45]. Furthermore, unlike in 1D the effect of dipolar interactions does not vanish at the magic angle  $\tilde{\theta}_m$ : while the dipolar contact interaction term vanishes, the nonlocal term [last term in Eq. (16a)] does not.

Analogous to the quasi-1D case, we now derive an approximate analytical expression for the density. To this end we assume that a repulsive contact interaction term (third term) in Eq. (16a) dominates the ground state solution. Hence, we neglect the kinetic and nonlocal terms in Eq. (16a). With the stationary ansatz  $\psi_{2D}(x, y, t) = e^{-i\mu_r t}\sqrt{n_{2D}(r)}$  we find the density profile  $n_{2D}(r) = [\mu_r - (r^2/2)]\{\beta_{2D}[1 - \frac{\epsilon_{dd}}{\sqrt{2\pi\gamma}}(1 - 3n_z^2)]\}^{-1}$ , where  $r^2 = x^2 + y^2$  and  $\mu_r$  is the radial part of the chemical potential. The density vanishes for  $r \geq R = \sqrt{2\mu_r}$ . By evaluating the normalization of the density,  $2\pi \int dr r n_{2D}(r) = 1$ , we find the mean-field radius

$$R = \left( \frac{4\beta_{2D}}{\pi\sqrt{2\pi\gamma}}[1 - \epsilon_{dd}(1 - 3n_z^2)] \right)^{1/4}. \quad (19)$$

Inserting this radius into the analytical density profile yields

$$n_{2D}(r) = \frac{2}{\pi R^2} \left( 1 - \frac{r^2}{R^2} \right). \quad (20)$$

For the special case  $n_z = 1$  our expression for the density  $n_{2D}(r)$  coincides with the expression for the ‘‘2D mean-field regime’’ given in Ref. [25]. We can formally generalize the condition for the validity of Eq. (20) given in Refs. [25, 48] to

$$\frac{\beta_{2D}\sqrt{\gamma^3}}{4\pi}[1 - \epsilon_{dd}(1 - 3n_z^2)] \ll 1. \quad (21)$$

While this condition may suggest that  $n_{2D}(r)$  is a good approximation for large dipole moment and small axial polarization  $n_z$ , we note that in the regime  $n_z \lesssim 1/\sqrt{3}$  the anisotropy and magnitude of the potential  $\Phi_{2D}$  increases appreciable.

This may be seen by evaluating the kernel  $U_{2D}^n$  given in Appendix C. In other words,  $n_{2D}(r)$  is a good approximation for the 2D density profile if condition Eq. (21) is fulfilled and the dipoles are polarized *predominantly* in the axial direction.

By numerically solving Eq. (16) we obtain radial density profiles of a quasi-2D dipolar BEC for various trap anisotropies and polarizations. For axial polarization ( $n_z = 1$ ) we find a radially symmetric density. For nonaxial polarization ( $n_z < 1$ ) we find that the quasi-2D BEC is elongated along the polarization axis projected onto the  $x$ - $y$  plane and compressed orthogonal to the polarization axis. This is in contrast to the quasi-1D case where the attraction between aligned dipoles compresses the BEC along the polarization axis. This is a result of the saddle shape of the potential  $U_{2D}^n$  with minima along the projection of the dipole axis. The experiments in Ref. [3, 49] show such an elongation of a dipolar BEC in the Thomas-Fermi regime.

In Fig. 4 we show density profiles of the quasi-2D BEC along the elongated (solid blue lines) and compressed axes (dashed red) in the  $x$ - $y$  plane. If the dipoles are aligned parallel to the symmetry axis of the quasi-2D BEC ( $n_z = 1$ ), the overall dipolar interaction is repulsive. This is manifest in Eq. (16), where the contact interaction term becomes larger for positive dipole strength  $\epsilon_{dd}$  and the nonlocal potential is positive. Moreover, the BEC remains radially symmetric as a result of the vanishing radially asymmetric derivative  $\partial_{\mathbf{n}_\perp\mathbf{n}_\perp}$ . We plot the radially symmetric density profile for  $n_z = 1$  in the top panel of Fig. 4. The radial profile of the BEC becomes increasingly asymmetric as we move the polarization away from the  $z$  axis. This is evident in the different widths of the density profiles along the two orthogonal axes in the middle and bottom panels of Fig. 4. The plots with polarizations along the  $x$  axis or the diagonal of the  $x$ - $y$  plane (middle and bottom left panel of Fig. 4) show the largest difference in width. The case of equal polarization in all directions (bottom right panel in Fig. 4),  $\mathbf{n} = \frac{1}{\sqrt{3}}(1, 1, 1)$ , is special because the dipole interaction does not have a local character. This is manifest in Eq. (16) where the contribution of the dipole interaction to the contact interaction vanishes at the angle  $n_z = \cos\tilde{\theta} \approx 54.7^\circ$ . Consequently, in the bottom right panel of Fig. 4 we only observe a very small asymmetry of the radial BEC density, which is a purely nonlocal effect caused by the potential  $\Phi_{2D}$ .

For comparison, in Fig. 4 we also plot the density profiles of a dipolar BEC obtained by numerically solving the 3D GPE, Eq. (1), and integrating over the  $z$  direction. We find excellent agreement with the solutions of our proposed 2D equations (16) for sufficiently large trap anisotropies. In the top left panel of Fig. 4 we notice a slight discrepancy to the 2D solution because the trap anisotropy is not sufficient to suppress the change in the axial density profile caused by the dipole interaction. Furthermore, in Fig. 4 we plot the approximation  $n_{2D}(r)$ , Eq. (20). We observe good agreement within its regime of validity discussed below Eq. (21). The analytical approximation of the radial profile agrees well with the numerical ground state solution if the polarization is predominantly perpendicular to the BEC disc (top and bottom right panels of Fig. 4). For polarizations predominantly in the

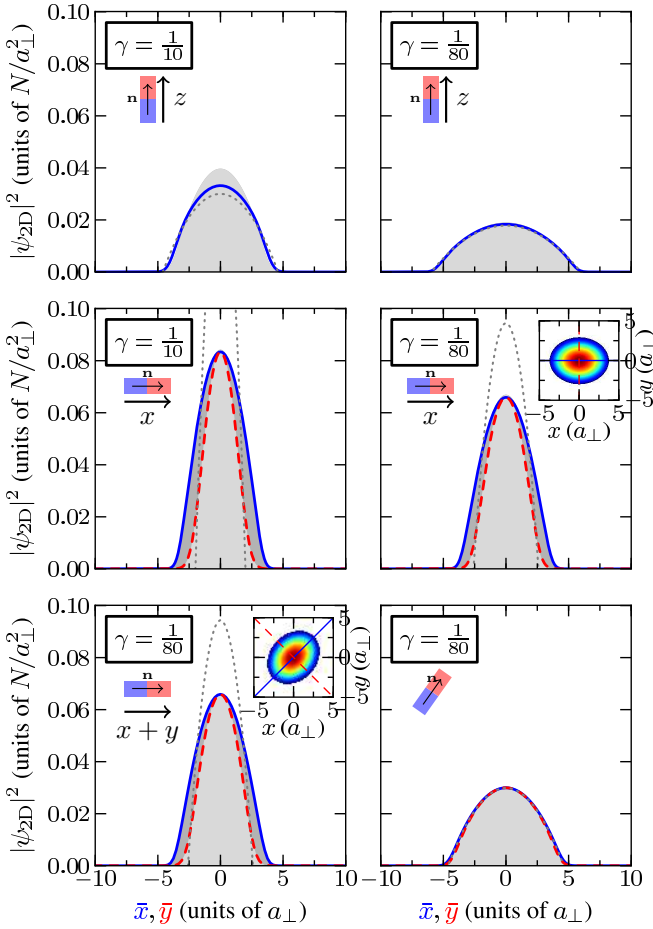


FIG. 4. (Color online) Cuts through the radial density profiles of the quasi-2D dipolar BEC given by Eq. (16) for various polarizations and trap anisotropies. The cuts are taken along the axes with largest ( $\bar{x}$  axis, solid blue lines) and smallest extend of the BEC ( $\bar{y}$  axis, dashed red). The insets show density plots of the quasi-2D BEC and the lines indicate the position of the cuts ( $\bar{x}$  and  $\bar{y}$  axes, respectively). The gray dotted lines are the analytical profiles  $n_{2D}(r)$  and the shaded areas are the profiles obtained from the 3D GPE, Eq. (1). For sufficiently large confinement the 3D GPE profiles are not distinguishable from our 2D solution. We choose  $\beta_{2D} = 100$ ,  $\epsilon_{dd} = 0.9$  and the dipole axis  $\mathbf{n} = (0, 0, 1)$  (top panel),  $\mathbf{n} = (1, 0, 0)$  (middle panel),  $\mathbf{n} = \frac{1}{\sqrt{2}}(1, 1, 0)$  (bottom left panel) and  $\mathbf{n} = \frac{1}{\sqrt{3}}(1, 1, 1)$  (bottom right panel).

plane of the quasi-2D BEC our proposed Eq. (16) remains a good approximation while the analytical approximation becomes invalid.

We have seen in Fig. 4 that the quasi-2D BEC in a radially symmetric trap loses its radial symmetry if the dipole axis does not point along its symmetry axis. This is a consequence of the anisotropic nature of the dipolar interaction. It is possible to observe this effect experimentally by measuring the aspect ratio

$$\frac{\sigma_y}{\sigma_x} = \frac{\sqrt{\langle y^2 \rangle}}{\sqrt{\langle x^2 \rangle}} \quad (22)$$

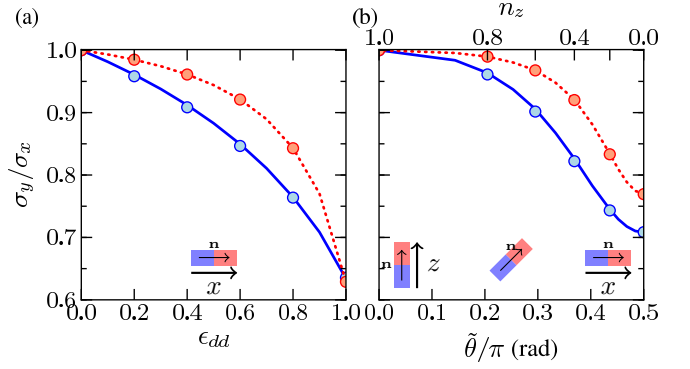


FIG. 5. (Color online) Aspect ratio of the quasi-2D BEC for (a) varying dipole strength  $\epsilon_{dd}$  with polarization along the  $x$  axis and (b) varying polarization angle in the  $x$ - $z$  plane [ $\mathbf{n} = (\sin \tilde{\theta}, 0, \cos \tilde{\theta})$ ] with  $\epsilon_{dd} = 0.9$ . We use the trap aspect ratios  $\gamma = 1/10$  (solid lines) and  $\gamma = 1/80$  (dotted) with  $\beta_{2D} = 100$ . The circles indicate the corresponding condensate aspect ratio according to the numerical solution the 3D GPE, Eq. (1). The upper axis in (b) shows  $n_z = \cos \tilde{\theta}$ .

of the BEC. The aspect ratio is particularly suited for measurements because it is not sensitive on the exact number of particles [40].

We have computed the aspect ratio of a dipolar BEC by numerically solving our 2D equations (16) for different values of the dipole moment and polarization angle. Fig. 5 summarizes these results. In Fig. 5(a) we plot the aspect ratio for polarization along the  $x$  axis and varying dipole interaction strength  $\epsilon_{dd}$ . We observe that the BEC becomes increasingly elongated as we increase the dipolar interaction strength. In Fig. 5(b) we fix the dipole strength but let the dipolar axis rotate in the  $x$ - $z$  plane. This shows how the radial BEC density profile changes from a symmetric disc to an oval shape as we rotate the polarization away from the  $z$  axis. We note that large changes in the aspect ratio occur in a region around the magic angle  $\tilde{\theta} \simeq \tilde{\theta}_m$ , where the effective contact interaction is nearly independent of the dipole interaction strength  $\epsilon_{dd}$ . Large trap anisotropies [dashed line in Fig. 5(b)] suppress the onset of significant BEC asymmetry because the contact interaction dominates the ground state. We have also obtained the aspect ratios by numerically solving the 3D GPE, Eq. (1) and integrating over the  $z$  axis (circles in Fig. 5). We find excellent agreement with the aspect ratios obtained from our 2D equations. Since a rotation of the polarization in the  $x$ - $y$  plane only corresponds to a rotation of the elongated axis of the ground state density (see Fig. 4), we obtain similar results to Fig. 5(b) for arbitrary polarization. This shows that the reduced Eqs. (16) are indeed a good approximation for describing quasi-2D dipolar BECs at arbitrary polarization with sufficiently strong axial trapping.

## V. CONCLUSION

We have presented Gross-Pitaevskii-type mean-field equations for trapped quasi-1D, Eq. (9), and quasi-2D, Eq. (16),

dipolar BECs polarized along an arbitrary axis. These equations are based on a rigorous dimension reduction of the full 3D GPE. In contrast to previous works, they are valid for arbitrary dipole alignment in the mean-field regime if the BEC is in the ground state of the radial or axial harmonic trap, respectively. Our result shows that quasi-1D and quasi-2D dipolar BECs are governed by a modified contact interaction term and an additional nonlocal potential. We have given explicit expressions for the nonlocal potential for arbitrary polarization (also see Appendix C).

One of the main advantages of the proposed mean-field equations is that they are well suited for numerical computations in strongly confined BECs. Our numerical implementations of the ground state computation in 1D and 2D perform much faster than our equivalent 3D computations. This is because we only need to integrate over the reduced dimensions, which vary over similar time scales, whereas the excluded dimensions vary on a much faster time scale for strong trap anisotropies. Moreover, the kernel of the convolution in the nonlocal potential is bounded in 1D and diverges only logarithmically in 2D. In contrast, in 3D the corresponding kernel diverges inverse linearly. Our formulation of the nonlocal potential in terms of partial derivatives allows for efficient numerical methods based on the Fourier transformation.

We have computed the ground states of our 1D and 2D equations numerically and compared them with the ground states of the 3D GPE. We find excellent agreement but notice small discrepancies in 1D for the case when the BEC is polarized perpendicular to the elongated direction. By neglecting the kinetic energy term and assuming a vanishing nonlocal potential we have derived analytical expressions for the density profiles of quasi-1D and quasi-2D dipolar BECs when the dipoles are aligned predominantly along the  $z$  axis. The ground state of the quasi-2D dipolar BEC becomes anisotropic if the polarization is not parallel to the symmetry axis of the pancake-shaped BEC. This results in a varying aspect ratio of the BEC pancake, which can be measured with time-of-flight imaging. We have computed this aspect ratio for varying dipole interaction strength, trap anisotropy and polarization axis.

As an outlook, we point out that it is straightforward to use our equations for studying the dynamics of arbitrarily polarized dipolar BECs in lower dimensions. They also allow for a stability analysis of such lower dimensional dipolar BECs. In a future work we will investigate the influence of a changing dipole axis on the formation of vortices in 2D dipolar BECs in a rotating frame.

## ACKNOWLEDGMENTS

We would like to thank Hanquan Wang for his help with some of the numerical computation. This work was supported by the Academic Research Fund of Ministry of Education of Singapore grant R-146-000-120-112. ZL acknowledges support in part by National Science Foundation of China (NSFC) grants 10801029 and 10911120384, FANEDD, Shanghai Rising Star Program (10QA1400300), SGST 09DZ2272900, and

SRF for ROCS-SEM.

## Appendix A: Derivation of the 1D mean-field equation

Under the assumption in Sec. III, plugging  $\psi(\mathbf{r}, t) = e^{-i\omega_{\perp}t}w_{2D}(x, y)\psi_{1D}(z, t)$  into the GPE, Eq. (6a), after rescaling, we have

$$i\partial_t\psi_{1D}w_{2D} = \left( \frac{-\partial_{zz} + z^2}{2} + \beta_1|\psi_{1D}w_{2D}|^2 + \partial_{\mathbf{nn}}\Phi \right) \psi_{1D}w_{2D}, \quad (\text{A1})$$

where

$$\Phi = -3\beta_{1D}\epsilon_{dd} \int d^3\mathbf{r}' U_{3D}(\mathbf{r} - \mathbf{r}') |(\psi_{1D}w_{2D})(\mathbf{r}', t)|^2 \quad (\text{A2})$$

with the rescaled quantities  $w_{2D}(x, y) = \sqrt{\frac{\gamma}{\pi}}e^{-\frac{\gamma}{2}(x^2+y^2)}$ ,  $\beta_1 = \beta_{1D}(1 - \epsilon_{dd})$ . By multiplying both sides of Eq. (A1) by  $w_{2D}(x, y)$  and integrating over the  $x$ - $y$  plane we obtain an equation in  $z$  only. Since  $w_{2D}(x, y)$  is normalized according to  $\int dx dy w_{2D}^2(x, y) = 1$  and  $\int dx dy w_{2D}^4(x, y) = \gamma/2\pi$ , this integration is straightforward for all but the last term. In the following we outline the calculation of this last term.

In order to obtain Eq. (9), we need to compute

$$\iint_{-\infty}^{\infty} dx dy \partial_{\mathbf{nn}}\Phi(x, y, z, t) w_{2D}^2(x, y). \quad (\text{A3})$$

Noticing the symmetry of  $U_{3D}$  and  $w_{2D}$  in  $x$  and  $y$  we see that

$$\partial_{xx}(U_{3D} * |\psi_{1D}w_{2D}|^2) = \partial_{yy}(U_{3D} * |\psi_{1D}w_{2D}|^2), \quad (\text{A4})$$

where we denote with  $a * b$  the convolution of  $a$  and  $b$ . Since  $U_{3D}$  is the Green's function of the Poisson equation [23], we have  $-\nabla^2 U_{3D}(\mathbf{r}) = \delta(\mathbf{r})$ . Inserting Eq. (A4) into this expression yields

$$\partial_{xx}(U_{3D} * |\psi_{1D}w_{2D}|^2) = -\frac{|\psi_{1D}w_{2D}|^2}{2} - \frac{\partial_{zz}(U_{3D} * |\psi_{1D}w_{2D}|^2)}{2}. \quad (\text{A5})$$

Moreover,  $|\psi_{1D}w_{2D}|^2$  is an even function with respect to  $x$  and  $y$  and so is  $U_{3D} * |\psi_{1D}w_{2D}|^2$ , which implies that the partial derivatives  $\partial_{xy}$ ,  $\partial_{yz}$ ,  $\partial_{xz}$  of  $U_{3D} * |\psi_{1D}w_{2D}|^2$  are odd functions in  $x$  and  $y$ . Recalling  $\partial_{\mathbf{nn}} = n_x^2\partial_{xx} + n_y^2\partial_{yy} + n_z^2\partial_{zz} + 2n_x n_y \partial_{xy} + 2n_y n_z \partial_{yz} + 2n_x n_z \partial_{xz}$  we plug Eq. (A5) into Eq. (A3), which yields

$$3\beta_{1D}\epsilon_{dd} \left( \frac{1 - n_z^2}{2} \frac{\gamma}{2\pi} |\psi_{1D}|^2 + \frac{1 - 3n_z^2}{2} \partial_{zz} \iint dx dy (U_{3D} * |\psi_{1D}w_{2D}|^2) w_{2D}^2 \right) \quad (\text{A6})$$

because integrals of odd functions (the mixed partial derivatives) vanish. We see that the first term in Eq. (A6) contributes to the modification of the contact interaction term in Eq. (9a).



In order to evaluate the last term in Eq. (A6) we expand the convolution and compute the resulting integrals

$$\int_{\mathbb{R}^4} dx' dy' dx dy \frac{w_{2D}^2(x', y') w_{2D}^2(x, y)}{4\pi \sqrt{(x-x')^2 + (y-y')^2 + (z-z')^2}}.$$

To this end, we introduce the variables  $\tilde{x} = x - x'$ ,  $\tilde{x}' = x + x'$ ,  $\tilde{y} = y - y'$ ,  $\tilde{y}' = y + y'$  and integrate over  $\tilde{x}'$  and  $\tilde{y}'$ . The result is

$$\iint d\tilde{x} d\tilde{y} \frac{\gamma e^{-\frac{\gamma}{2}(\tilde{x}^2 + \tilde{y}^2)}}{8\pi^2 \sqrt{\tilde{x}^2 + \tilde{y}^2 + (z-z')^2}}, \quad (\text{A7})$$

which can be evaluated further in polar coordinates  $\tilde{x} = r \cos \theta'$ ,  $\tilde{y} = r \sin \theta'$ . Equation (A7) reduces to  $\frac{\sqrt{\gamma}}{4\sqrt{2\pi}} U_{1D}(z - z')$  with the substitution  $\zeta = \sqrt{r^2 + (z - z')^2}$  and

$$U_{1D}(z) = \sqrt{\frac{2\gamma}{\pi}} e^{\gamma z^2/2} \int_{|z|}^{\infty} d\zeta e^{-\gamma \zeta^2/2}. \quad (\text{A8})$$

Equation (A8) is an integral representation of  $U_{1D}$  given in Eq. (10). Inserting Eq. (A8) back into Eq. (A6) we obtain the potential  $\Phi_{1D}$ , Eq. (9b). Plugging Eq. (A6) into the integrated Eq. (A1) results in the mean-field equation for a quasi-1D dipolar BEC, Eq. (9).

The Fourier transform of  $U_{1D}(z)$  is given by

$$\widehat{U}_{1D}(k_z) = \frac{1}{\sqrt{\gamma\pi}} \int_0^{\infty} dk \frac{e^{-\frac{\kappa}{2\gamma}}}{k_z^2 + \kappa}. \quad (\text{A9})$$

The asymptotic behavior of this Fourier transform is  $\widehat{U}_{1D}(k_z) = \frac{1}{\sqrt{\gamma\pi}} [\ln(2\gamma) - \gamma_e - 2 \ln |k_z|] + \mathcal{O}(k_z)$  for  $|k_z| \rightarrow 0$  and  $\widehat{U}_{1D}(k_z) \sim \frac{2\sqrt{\gamma}}{\pi} \frac{1}{|k_z|^2}$  for  $|k_z| \rightarrow \infty$ , where  $\gamma_e$  is the Euler-Mascheroni constant.

## Appendix B: Derivation of the 2D mean-field equation

Under the assumptions in Sec. IV, plugging  $\psi(\mathbf{r}, t) = e^{-i\omega_z t/2} w_{1D}(z) \psi_{2D}(x, y, t)$  into the GPE, Eq. (6a), after rescaling, we have

$$i\partial_t \psi_{2D} w_{1D} = \left\{ \frac{-\nabla_{\perp}^2 + V_{2D}}{2} + \beta_2 |\psi_{2D} w_{1D}|^2 + \partial_{\mathbf{nn}} \Phi \right\} \psi_{2D} w_{1D}, \quad (\text{B1})$$

where now

$$\Phi = -3\beta_{2D} \epsilon_{dd} \int d^3 \mathbf{r}' U_{3D}(\mathbf{r} - \mathbf{r}') |\psi_{2D} w_{1D}(\mathbf{r}', t)|^2, \quad (\text{B2})$$

with rescaled  $w_{1D}(z) = \left(\frac{1}{\gamma\pi}\right)^{1/4} e^{-\frac{z^2}{2\gamma}}$ ,  $\nabla_{\perp}^2 = \partial_{xx} + \partial_{yy}$ ,  $\beta_2 = \beta_{2D}(1 - \epsilon_{dd})$ . Multiplying both sides of Eq. (B1) by  $w_{1D}(z)$  and integrating over the  $z$  direction, we can obtain a 2D wave equation for  $\psi_{2D}$ .

As in the preceding appendix, the integration is straightforward for all but the last term because  $\int dz w_{1D}^2(z) = 1$  and

$\int dz w_{1D}^4(z) = 1/\sqrt{2\pi\gamma}$ . In the following we only present the integration of the last term of Eq. (B1),

$$\int_{-\infty}^{\infty} dz \partial_{\mathbf{nn}} \Phi(x, y, z, t) w_{1D}^2(z). \quad (\text{B3})$$

Again we use the identity  $-\nabla^2 U_{3D}(\mathbf{r}) = \delta(\mathbf{r})$  to write

$$\begin{aligned} \partial_{zz} (U_{3D} * |\psi_{2D} w_{1D}|^2) &= -|\psi_{2D} w_{1D}|^2 \\ &\quad - \nabla_{\perp}^2 (U_{3D} * |\psi_{2D} w_{1D}|^2). \end{aligned}$$

We recall that  $|\psi_{2D}(x, y, t) w_{1D}(z)|^2$  is even in  $z$  so that  $U^{3D} * |\psi_{2D} w_{1D}|^2$  also becomes even in  $z$  and  $\partial_{\mathbf{n}_{\perp} z} (U^{3D} * |\psi_{2D} w_{1D}|^2)$  becomes odd in  $z$ . Plugging  $\partial_{\mathbf{nn}} = \partial_{\mathbf{n}_{\perp} \mathbf{n}_{\perp}} + n_z^2 \partial_{zz} + 2n_z \partial_{\mathbf{n}_{\perp} z}$  into Eq. (B3) yields

$$\begin{aligned} &3\beta_{2D} \epsilon_{dd} \left( \frac{n_z^2}{\sqrt{2\gamma\pi}} |\psi_{2D}|^2 \right. \\ &\quad \left. - (\partial_{\mathbf{n}_{\perp} \mathbf{n}_{\perp}} - n_z^2 \nabla_{\perp}^2) \int_{-\infty}^{\infty} dz (U_{3D} * |\psi_{2D} w_{1D}|^2) w_{1D}^2(z) \right), \end{aligned} \quad (\text{B4})$$

where the  $\partial_{\mathbf{n}_{\perp} z}$  term disappears because the integral of odd functions vanishes. The first term in Eq. (B4) contributes to the modified contact interaction term in Eq. (16).

After expanding the convolution in the last term of Eq. (B4), we see that we need to compute the integral

$$\iint_{-\infty}^{\infty} dz' dz \frac{w_{1D}^2(z') w_{1D}^2(z)}{4\pi \sqrt{(x-x')^2 + (y-y')^2 + (z-z')^2}}. \quad (\text{B5})$$

By changing the variables according to  $\tilde{z} = z - z'$ ,  $\tilde{z}' = z + z'$ , and integrating over  $\tilde{z}'$  we reduce Eq. (B5) to

$$\int_{-\infty}^{\infty} d\tilde{z} \frac{1}{2\sqrt{\gamma}(2\pi)^{3/2}} \frac{e^{-\tilde{z}^2/2\gamma}}{\sqrt{(x-x')^2 + (y-y')^2 + \tilde{z}^2}}. \quad (\text{B6})$$

By substituting  $\rho = \tilde{z}/\sqrt{\gamma}$  and introducing polar coordinates with  $r = \sqrt{(x-x')^2 + (y-y')^2}$  we get

$$U_{2D}(r) = \frac{1}{(2\pi)^{3/2}} \int_{-\infty}^{\infty} d\rho \frac{e^{-\rho^2/2}}{\sqrt{r^2 + \gamma\rho^2}}. \quad (\text{B7})$$

This integral representation of  $U_{2D}(r)$  is identical to Eq. (17) [50, see Sec. 3.364]. We obtain the potential  $\Phi_{2D}$ , Eq. (16b), from the last term in Eq. (B4) after inserting Eq. (B7). Finally, plugging Eq. (B4) into the integrated Eq. (B1) results in the mean-field equation for the quasi-2D dipolar BEC, Eq. (16).

The Fourier transform  $\widehat{U}_{2D}(k_x, k_y)$  of the radially symmetric kernel  $U_{2D}$  is also radially symmetric and given by

$$\widehat{U}_{2D}(|k_r|) = \frac{1}{2\pi^2} \int_{-\infty}^{\infty} dk \frac{e^{-\frac{\gamma k^2}{2}}}{|k_r|^2 + \kappa^2} \quad (\text{B8})$$

with  $|k_r| = \sqrt{k_x^2 + k_y^2}$ . The asymptotic behavior of this Fourier transform is  $\widehat{U}_{2D}(|k_r|) \sim \frac{1}{2\pi|k_r|}$  for  $|k_r| \rightarrow 0$  and  $\widehat{U}_{2D}(|k_r|) \sim \frac{1}{\sqrt{2\pi^3\gamma}} \frac{1}{|k_r|^2}$  for  $|k_r| \rightarrow \infty$ .

### Appendix C: Closed forms of the 1D and 2D nonlocal potentials

In this appendix, we derive closed forms for the nonlocal potentials  $\Phi_{1D}$ , Eq. (9b), and  $\Phi_{2D}$ , Eq. (16b). Owing to the properties of the convolution in  $\Phi_{1D}$  we may write Eq. (9b) as

$$\Phi_{1D} = \frac{3\beta_{1D}\epsilon_{dd}\sqrt{\gamma}}{8\sqrt{2\pi}}(1 - 3n_z^2)(\partial_{zz}U_{1D}) * |\psi_{1D}|^2,$$

*i.e.*, the derivatives only affect the kernel  $U_{1D}$ . Straightforward calculation of the second derivative of Eq. (10) leads to

$$\tilde{U}_{1D}(z) = \partial_{zz}U_{1D}(z) = \gamma U_{1D}(z)(1 + \gamma z^2) - \sqrt{\frac{2\gamma^3}{\pi}}|z|.$$

The resulting nonlocal potential  $\Phi_{1D}$  is of the same form as the one given in Ref. [27] for the special case of axial polarization.

$$U_{2D}^{(n)}(x, y) = \frac{e^{r^2/4\gamma}}{2(2\pi\gamma)^{3/2}} \left[ \left( 1 - 3n_z^2 + \frac{(n_x x + n_y y)^2 - n_z^2 r^2}{\gamma} \right) K_0 - \left( 1 - n_z^2 + \frac{(n_x x + n_y y)^2 [1 - 2\gamma/r^2] - n_z^2 r^2}{\gamma} \right) K_1 \right] \quad (C2)$$

and the nonlocal potential  $\Phi_{2D} = -\frac{3\beta_{2D}\epsilon_{dd}}{2}U_{2D}^{(n)} * |\psi_{2D}|^2$ . The kernel  $U_{2D}^{(n)}(x, y)$  changes from a symmetric peak for  $n_z = 1$  to a saddle shape with minima along the projection of the dipole axis onto the  $x$ - $y$  plane for  $n_z < 1$ . We note that

In an analogous fashion,  $\Phi_{2D}$  in Eq. (16b) is given by

$$\Phi_{2D} = -\frac{3\beta_{2D}\epsilon_{dd}}{2} [(\partial_{\mathbf{n}_\perp \mathbf{n}_\perp} - n_z^2 \nabla^2) U_{2D}] * |\psi_{2D}|^2. \quad (C1)$$

By using Eq. (17) and the properties of the derivatives of Bessel functions we find for the second derivatives of  $U_{2D}$

$$\begin{aligned} \partial_{xx}^2 U_{2D} &= \frac{e^{r^2/4\gamma}}{2(2\pi\gamma)^{3/2}} \left[ \left( 1 + \frac{x^2}{\gamma} \right) K_0 - \left( 1 + \frac{x^2}{\gamma} - \frac{2x^2}{r^2} \right) K_1 \right], \\ \partial_{yy}^2 U_{2D} &= \frac{e^{r^2/4\gamma}}{2(2\pi\gamma)^{3/2}} \left[ \left( 1 + \frac{y^2}{\gamma} \right) K_0 - \left( 1 + \frac{y^2}{\gamma} - \frac{2y^2}{r^2} \right) K_1 \right], \\ \partial_{xy}^2 U_{2D} &= \partial_{yx}^2 U_{2D} = \frac{e^{r^2/4\gamma}}{2(2\pi\gamma)^{3/2}} \left[ \frac{xy}{\gamma} K_0 - \left( \frac{xy}{\gamma} - \frac{2xy}{r^2} \right) K_1 \right]. \end{aligned}$$

Here and in the following we suppress the argument  $r^2/4\gamma$  of the Bessel functions with  $r^2 = x^2 + y^2$ . Plugging these identities into Eq. (C1) we find for the nonlocal kernel  $U_{2D}^{(n)}(x, y) = (\partial_{\mathbf{n}_\perp \mathbf{n}_\perp} - n_z^2 \nabla^2) U_{2D}(r)$

$\Phi_{2D}$  reduces to the potential for axial polarization ( $n_z = 1$ ) derived, *e.g.*, in Ref. [31]. However, Eq. (C2) is valid for arbitrary polarization.

- 
- [1] L. Pitaevskii and S. Stringari, *Bose-Einstein Condensation* (Oxford University Press, Oxford, 2003).
- [2] A. Griesmaier, J. Werner, S. Hensler, J. Stuhler, and T. Pfau, *Phys. Rev. Lett.* **94**, 160401 (2005).
- [3] J. Stuhler, A. Griesmaier, T. Koch, M. Fattori, T. Pfau, S. Giovanazzi, P. Pedri, and L. Santos, *Phys. Rev. Lett.* **95**, 150406 (2005).
- [4] K. Góral, K. Rzążewski, and T. Pfau, *Phys. Rev. A* **61**, 051601 (2000).
- [5] S. Yi and L. You, *Phys. Rev. A* **61**, 041604 (2000).
- [6] L. Santos, G. V. Shlyapnikov, P. Zoller, and M. Lewenstein, *Phys. Rev. Lett.* **85**, 1791 (2000).
- [7] L. Santos, G. V. Shlyapnikov, and M. Lewenstein, *Phys. Rev. Lett.* **90**, 250403 (2003).
- [8] S. Yi and L. You, *Phys. Rev. A* **63**, 053607 (2001).
- [9] H. P. Büchler, E. Demler, M. Lukin, A. Micheli, N. Prokof'ev, G. Pupillo, and P. Zoller, *Phys. Rev. Lett.* **98**, 060404 (2007).
- [10] K. Góral, L. Santos, and M. Lewenstein, *Phys. Rev. Lett.* **88**, 170406 (2002).
- [11] A. Micheli, G. K. Brennen, and P. Zoller, *Nat. Phys.* **2**, 341 (2006).
- [12] T. Lahaye, C. Menotti, L. Santos, M. Lewenstein, and T. Pfau, *Rep. Prog. Phys.* **72**, 126401 (2009).
- [13] M. A. Baranov, *Phys. Rep.* **464**, 71 (2008).
- [14] T. Koch, T. Lahaye, J. Metz, B. Fröhlich, A. Griesmaier, and T. Pfau, *Nat. Phys.* **4**, 218 (2008).
- [15] M. Fattori, G. Roati, B. Deissler, C. D'Errico, M. Zaccanti, M. Jona-Lasinio, L. Santos, M. Inguscio, and G. Modugno, *Phys. Rev. Lett.* **101**, 190405 (2008).
- [16] M. Vengalattore, S. R. Leslie, J. Guzman, and D. M. Stamper-Kurn, *Phys. Rev. Lett.* **100**, 170403 (2008).
- [17] M. Marinescu and L. You, *Phys. Rev. Lett.* **81**, 4596 (1998).
- [18] C. Haimberger, J. Kleinert, M. Bhattacharya, and N. P. Bigelow, *Phys. Rev. A* **70**, 021402 (2004).
- [19] J. M. Sage, S. Sainis, T. Bergeman, and D. DeMille, *Phys. Rev. Lett.* **94**, 203001 (2005).
- [20] K. Ni, S. Ospelkaus, M. H. G. de Miranda, A. Pe'er, B. Neyenhuis, J. J. Zirbel, S. Kotochigova, P. S. Julienne, D. S. Jin, and J. Ye, *Science* **322**, 231 (2008).
- [21] S. Ospelkaus, A. Pe'er, K. Ni, J. J. Zirbel, B. Neyenhuis, S. Kotochigova, P. S. Julienne, J. Ye, and D. S. Jin, *Nat. Phys.* **4**, 622 (2008).
- [22] T. Vogt, M. Viteau, J. Zhao, A. Chotia, D. Comparat, and P. Pillet, *Phys. Rev. Lett.* **97**, 083003 (2006).
- [23] D. H. J. O'Dell, S. Giovanazzi, and C. Eberlein, *Phys. Rev. Lett.* **92**, 250401 (2004).

- [24] C. Eberlein, S. Giovanazzi, and D. H. J. O'Dell, *Phys. Rev. A* **71**, 033618 (2005).
- [25] N. G. Parker and D. H. J. O'Dell, *Phys. Rev. A* **78**, 041601 (2008).
- [26] S. Giovanazzi and D. H. J. O'Dell, *Euro. Phys. J. D* **31**, 439 (2004).
- [27] S. Sinha and L. Santos, *Phys. Rev. Lett.* **99**, 140406 (2007).
- [28] P. Pedri and L. Santos, *Phys. Rev. Lett.* **95**, 200404 (2005).
- [29] R. Nath, P. Pedri, and L. Santos, *Phys. Rev. Lett.* **102**, 050401 (2009).
- [30] S. Yi and H. Pu, *Phys. Rev. A* **73**, 061602 (2006).
- [31] S. Komineas and N. R. Cooper, *Phys. Rev. A* **75**, 023623 (2007).
- [32] W. Bao and W. J. Tang, *J. Comput. Phys.* **187**, 230 (2003).
- [33] W. Bao, D. Jaksch, and P. A. Markowich, *J. Comput. Phys.* **187**, 318 (2003).
- [34] L. Salasnich, *J. Phys. A: Math. Theor.* **42**, 335205 (2009).
- [35] N. B. Abdallah, F. Méhats, C. Schmeiser, and R. Weishäupl, *SIAM J. Math. Anal.* **37**, 189 (2005).
- [36] N. B. Abdallah, F. Castella, and F. Méhats, *J. Differential Equations* **245**, 154 (2008).
- [37] E. H. Lieb, R. Seiringer, and J. Yngvason, *Phys. Rev. Lett.* **91**, 150401 (2003).
- [38] J. Yngvason, E. H. Lieb, and R. Seiringer, *Commun. Math. Phys.* **244**, 347 (2004).
- [39] R. Carles, P. A. Markowich, and C. Sparber, *Nonlinearity* **21**, 2569 (2008).
- [40] S. Giovanazzi, A. Görlitz, and T. Pfau, *J. Phys. B* **5**, S208 (2003).
- [41] B. Deb and L. You, *Phys. Rev. A* **64**, 022717 (2001).
- [42] S. Giovanazzi, A. Görlitz, and T. Pfau, *Phys. Rev. Lett.* **89**, 130401 (2002).
- [43] W. Bao, Y. Cai, and H. Wang, *J. Comput. Phys.* **229**, 7874 (2010).
- [44] A. Görlitz, J. M. Vogels, A. E. Leanhardt, C. Raman, T. L. Gustavson, J. R. Abo-Shaeer, A. P. Chikkatur, S. Gupta, S. Inouye, T. Rosenband, and W. Ketterle, *Phys. Rev. Lett.* **87**, 130402 (2001).
- [45] D. S. Petrov, G. V. Shlyapnikov, and J. T. M. Walraven, *Phys. Rev. Lett.* **85**, 3745 (2000).
- [46] M. Olshanii, *Phys. Rev. Lett.* **81**, 938 (1998).
- [47] M. Mehring, *Principles of high resolution NMR in solids* (Springer, Berlin, 1983).
- [48] A. Muñoz Mateo and V. Delgado, *Phys. Rev. A* **77**, 013617 (2008).
- [49] T. Lahaye, T. Koch, B. Fröhlich, M. Fattori, J. Metz, A. Griesmaier, S. Giovanazzi, and T. Pfau, *Nature* **448**, 672 (2007).
- [50] I. S. Gradshteyn and I. M. Ryzhik, *Table of integrals, series, and products*, sixth ed., edited by A. Jeffrey and D. Zwillinger (Academic Press, San Diego, CA, 2000).